Macroporous p-Type Silicon Fabry−Perot Layers. Fabrication, Characterization, and Applications in Biosensing

Andreas Janshoff,[†] Keiki-Pua S. Dancil,[‡] Claudia Steinem,[†] Douglas P. Greiner,[‡] Victor S.-Y. Lin,[†] Christian Gurtner,[‡] Kianoush Motesharei,[†] Michael J. Sailor,*[,‡] and M. Reza Ghadiri*[,†]

Contribution from the Department of Chemistry & Molecular Biology and The Skaggs Institute for Chemical Biology, The Scripps Research Institute, La Jolla, California 92037, and Department of Chemistry and Biochemistry, University of California, San Diego, La Jolla, California 92093-0358

Received July 24, 1998

Abstract: We present in this paper that porous silicon can be used as a large surface area matrix as well as the transducer of biomolecular interactions. We report the fabrication of heavily doped p-type porous silicon with pore diameters that can be tuned, depending on the etching condition, from approximately 5 to 1200 nm. The structure and porosity of the matrixes were characterized by scanning force microscopy (SFM) and scanning electron microscopy (SEM), Brunnauer−Emmett−Teller nitrogen adsorption isotherms, and reflectance interference spectroscopy. The thin porous silicon layers are transparent to the visible region of the reflectance spectra due to their high porosity (80−90%) and are smooth enough to produce Fabry−Perot fringe patterns upon white light illumination. Porous silicon matrixes were modified by ozone oxidation, functionalized in the presence of (2-pyridyldithiopropionamidobutyl)dimethylmethoxysilane, reduced to unmask the sulfhydryl functionalities, and coupled to biotin through a disulfide-bond-forming reaction. Such functionalized matrixes display considerable stability against oxidation and corrosion in aqueous media and were used to evaluate the utility of porous silicon in biosensing. The streptavidin−biotin interactions on the surface of porous silicon could be monitored by the changes in the effective optical thickness calculated from the observed shifts in the Fabry−Perot fringe pattern caused by the change in the refractive index of the medium upon protein−ligand binding. Porous silicon thus combines the properties of a mechanically and chemically stable high surface area matrix with the function of an optical transducer and as such may find utility in the fabrication of biosensor devices.

Introduction

Since the early studies of Ulhir, Turner, and later Canham, porous silicon has been widely investigated for electronics, optoelectronics, and sensor applications.[1] Porous silicon can be prepared by chemical or electrochemical etching processes and consists of nano- or microcrystalline domains with defined pore morphologies. The diameter, geometric shape, and direction of the pores depend on surface orientation, doping level and type, temperature, the composition of the etching solution, and the current density.[2,3] Porous silicon has been employed as a large surface area matrix for immobilization of a variety of biomolecules including enzymes,[4] DNA fragments,[5] and antibodies.[6] Moreover, we recently showed that the electronic or optical properties of porous silicon can also be used as the transducer of biomolecular interactions, thus qualifying its utility in biosensor applications.[7,8] A Fabry−Perot fringe pattern is created by multiple reflections of illuminated white light on the air−porous silicon layer and the porous silicon−bulk silicon interface. The induced shift in the Fabry−Perot fringe pattern caused by the change in the refractive index of the medium upon molecular interactions of species in solution with immobilized ligands or receptors within the porous silicon matrix can be used as a sensitive method for biomolecular sensing.

The prerequisite for using porous silicon as an optical interferometric biosensor is to adjust the size as well as the geometrical shape of the pores by choosing the appropriate etching parameters. The pore size has to be large enough to allow biomolecules to enter the pores freely[9] but small enough to retain optical reflectivity of the porous silicon surface. Moreover, it is necessary that the material be mechanically and chemically stable in aqueous solutions to provide reproducible and predictable binding signals. Here we present the fabrication, characterization, and application of a porous silicon biosensor using highly doped p-type silicon wafers. Transparent porous

* To whom correspondence should be addressed.
† The Scripps Research Institute.
‡ University of California.

(1) (a) Ulhir, A. *Bell Syst. Tech. J.* **1956**, *35*, 333. (b) Turner, T. R. *J. Electrochem. Soc.* **1958**, *105*, 402. (c) Canham, P. C. *Appl. Phys. Lett.* **1990**, *57*, 1046. (d) Berger, M. G.; Arens-Fischer, R.; Thönissen, M.; Krüger, M.; Billat, S.; Lüth, H.; Hilbrich, S.; Theiss, W.; Grosse, P. *Thin Solid Films* **1997**, *297*, 237. (e) Cullis, A. G.; Canham, L. T.; Calcott, P. D. J. *J. Appl. Phys.* **1997**, *82*, 909.

(2) Smith, R. L.; Collins, S. D. *J. Appl. Phys.* **1992**, *71*, R1.

(3) Searson, P. C. *Advances in Electrochemical Sciences and Engineering*; VCH: Mannheim, Germany, 1994; p 69.

(4) (a) Drott, J.; Lindstrom, K.; Rosengren, L.; Laurell, T. *J. Micromech. Microeng.* **1997**, *7*, 14. (b) Thust, M.; Schoning, M. J.; Frohnhoff, S.; Arens-Fischer, R.; Cordos, P.; Luth, H. *Meas. Sci. Technol.* **1996**, *7*, 26.

(5) Beattie, K. L.; Beattie, W. G.; Meng, L.; Turner, S. L.; Coral-Vazquez, R.; Smith, D. D.; McIntyre, P. M.; Dao, D. D. *Clin. Chem.* **1995**, *41*, 700.

(6) Laurell, T.; Drott, J.; Rosengren, L.; Lindstrom, K. *Sens. Actuators, B* **1996**, *31*, 161.

(7) Lin, V. S.-Y.; Motesharei, K.; Dancil, K.-P. S.; Sailor, M. J.; Ghadiri, M. R. *Science* **1997**, *278*, 840.

(8) Sailor, M. J. *Properties of porous silicon*; Datareview Ser. No. 18; Canham: London, 1997; pp 364−370.

(9) Leyva-Ramos, R.; Geankoplis, C. J. *Chem. Eng. Sci.* **1985**, *40*, 799.

10.1021/ja9826237 CCC: $15.00 © 1998 American Chemical Society
Published on Web 11/04/1998

silicon thin films with large surface areas were prepared to give, depending on the fabrication conditions employed, a wide range of pore sizes. The pore size and the structure of the porous silicon layer were characterized using scanning force microscopy (SFM) and scanning electron microscopy (SEM). Reflectance interference spectroscopy and effective medium approximations were used to determine the porosity and the thickness of the porous layer. Appropriately functionalized porous silicon matrixes displayed the desired stability in aqueous solutions and were used to study specific protein−ligand binding interactions.

Results and Discussion

Fabrication and Characterization of p-Type Porous Silicon Interference Layers. The pore shape, pore size, and orientation of porous silicon layers depend on the surface orientation and the dopant level of the crystalline silicon substrate, the current density, the temperature, and the composition of the HF etching solution. Recently Hérino[10] reported the fabrication of macropores with diameters in the range 25−100 nm by anodizing heavily doped porous p-type silicon with a resistivity of 10^{-3} Ω cm in 25% ethanolic HF solution. Rieger and Kohl[11] have also shown that etching p-type silicon in dry solvents such as acetonitrile or DMF in a moisture-free environment leads to the formation of macroporous p-type silicon layers. We have extensively studied various parameters in the fabrication of porous silicon (vide infra). p-Type silicon with resistivities of 0.1−10 Ω cm etched in aqueous or ethanolic HF solutions generally displays a network of micropores (diameter d < 2 nm), rather than the desired well-defined cylindrical meso- (d = 2−50 nm) or macropores (d > 50 nm). However, the pore size of p-type porous silicon can be increased by increasing the concentration of the dopant and decreasing the aqueous HF concentration, but low current densities result in a random orientation of highly interconnected filament-like micropores. Large and cylindrically shaped pores can be obtained when higher current densities are applied near the electropolishing region. Our studies detailed below indicate that porous silicon layers can be fabricated to give cylindrically shaped structures with pore diameters in the tunable range of 5 to 1200 nm by anodizing heavily doped (10^{-3} Ω cm) p-type silicon (100) in ethanolic HF solution at ambient temperatures.

Scanning Force Microscopy. Scanning force microscopy was used to determine topographical parameters of the porous surface, such as surface porosity, pore size, and roughness.[12] TappingMode was used in this study since the surfaces of the porous layers were too fragile to be imaged in contact mode SFM.[13] The SFM images of samples obtained by etching silicon at different current densities are shown in Figure 1. Using relatively low current densities (150 mA/cm^2), pores are scarcely visible and the nearly flat surface is dominated by a distinct hillock structure (Figure 1A). According to Campbell et al.,[14] the hillocks are due to collapsed nanopores formed in the early stages of the etching process caused by disturbing the equilibrium lattice forces in the crystal, introducing a lateral strain in the surface layer. As the current densities are increased larger pore sizes can be obtained (Figure 1). The root mean square of the surface roughness is in the range 0.3−0.5 nm for porous silicon layers etched at current densities <200 mA/cm^2, which is in good agreement with a recent study by Yau et al.[15] The surface roughness was only determined for samples etched at current densities less than 200 mA/cm^2 because the macropores generated at higher current densities prevent an accurate measurement of this parameter with SFM.[16]

The pore radius is approximately exponentially dependent on the current density (Figure 2). The three smallest pore radii obtained at low current densities in the plot presented in Figure 2 were obtained from the BJH (Barett−Joyner−Halenda) calculation[17] while the rest of the values were derived from SFM measurements. The pore radii vary from 4−12 nm for samples etched at 220 mA/cm^2 up to 300−800 nm for samples etched at 600 mA/cm^2. The surface porosity of silicon layers etched at current densities larger than 300 mA/cm^2 was calculated from the SFM images by integrating the number of pixels. The surface porosity increases slightly from 27% with etching at 330 mA/cm^2 to 30% with etching at 410 mA/cm^2 and finally up to 40% by applying current densities >440 mA/cm^2. The artifact arising from the tip convoluting with the shape of the sample structure prevents accurate measurements of the surface porosity at higher current densities.

It is difficult to obtain reliable information about the pore size from samples with pores smaller than 5 nm because in this size regime the apparent pore size strongly depends on the shape of the SFM probe and the threshold height chosen. Imaging the large macropores (d > 800 nm) can result in unstable scans because the tip loses contact with the surface over a relatively long distance. In general, the pore sizes obtained from SFM images are slightly smaller than they are in reality. In particular, the walls of the large macropores have a rounded appearance due to the predominant interaction of the side of the tip with the pore walls.

Scanning Electron Microscopy. Scanning electron micrographs also corroborate the results obtained by TappingMode-SFM (see Supporting Information). In general, the images show similar meso/macroporous structures and pore sizes compared to the SFM images. Small surface features such as the hillock structures observed in Figure 1A could not be resolved by scanning electron microscopy (SEM). The SEM images of the samples etched at high current densities (>500 mA/cm^2) exhibit larger pore dimensions than the SFM images due to the geometric convolution between the tip and the walls of the large pores.

Generally the material investigated in this study follows the trend proposed by Smith and Collins[2] and Beale et al.[18] Anodization of the more highly doped p-type silicon leads to larger and more cylindrically shaped pores compared to the filament-like interconnected pores obtained using lightly doped p-type silicon. Furthermore, as suggested by the study of

(10) Hérino, R. *Properties of porous silicon*; Datareview Ser. No. 18; Canham: London, 1997; pp 89−96.

(11) Rieger, M. M.; Kohl, P. A. *J. Electrochem. Soc.* **1995**, *142*, 1490.

(12) (a) Sassaki, R. M.; Douglas, R. A.; Kleinke, M. U.; Teschke, O. *J. Vac. Sci. Technol. B* **1996**, *14*, 2432. (b) Enachescu, M.; Hartmann, E.; Koch, F. *Appl. Phys. Lett.* **1994**, *64*, 1365. (c) Zheng, D. W.; Huang, Y. P.; He, Z. J.; Li, A. Z.; Tang, T. A. *J. Appl. Phys.* **1997**, *81*, 492. (d) Parkhuitik, V. P.; Albella, J. M.; Martinez-Duart, J. M.; Gómez-Rodríguez, J. M.; Baró, A. M.; Shershulsky, V. I. *Appl. Phys. Lett.* **1993**, *62*, 366. (e) Amisola, G. B.; Behrensmeier, R.; Galligan, J. M.; Otter, F. A.; Namavar, F.; Kalkoran, N. M. *J. Vac. Sci. Technol. B* **1993**, *11*, 1788.

(13) Aktsipetrov, O. A.; Melnikov, A. V.; Moiseev, Y. N.; Murzina, T. V.; van Hasselt, C. W.; Rasing, T.; Rikken, G. *Appl. Phys. Lett.* **1995**, *67*, 1191.

(14) Campbell, S. D.; Jones, L. A.; Nakamichi, E.; Wei, F. X.; Zajchowski, L. D.; Thomas, D. F. *J. Vac. Sci. Technol., B* **1995**, *13*, 1184.

(15) Yau, S.-L.; Arendt, M.; Bard, A. J.; Evans, B.; Tsai, C.; Sarathy, J.; Campbell, J. C. *J. Electrochem. Soc.* **1994**, *2*, 402.

(16) Since the shape of the tip determines the penetration depth in the pores, the parameter would be tip dependent.

(17) Gregg, S. J.; Sing, K. S. W. *Adsorption, surface area and porosity*, 2nd ed.; Academic Press: New York, 1982.

(18) Beale, M. I. J.; Benjamin, M. J.; Uren, M. J.; Chew, N. G.; Cullis, A. G. *J. Cryst. Growth* **1985**, *73*, 622.

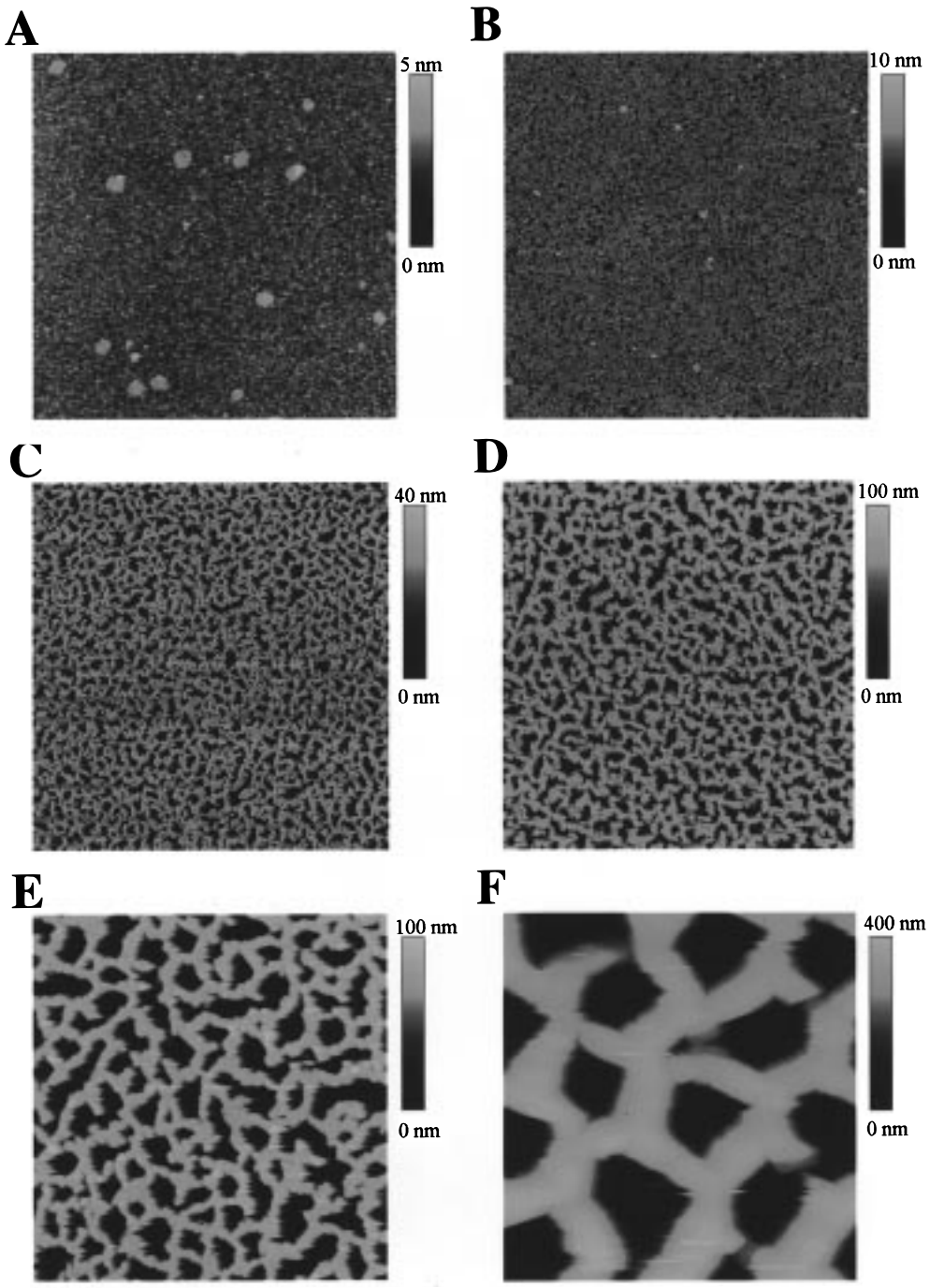

Figure 1. SFM images of freshly etched porous p-silicon layers etched at different current densities: (A) 1.5 × 1.5 μm^2 image etched at 150 mA/cm^2; (B) 5 × 5 μm^2 image etched at 295 mA/cm^2; (C) 5 × 5 μm^2 image etched at 370 mA/cm^2; (D) 5 × 5 μm^2 image etched at 440 mA/cm^2; (E) 5 × 5 μm^2 image etched at 515 mA/cm^2; (F) 5 × 5 μm^2 image etched at 600 mA/cm^2. The dopant concentration (1.0 mΩ cm) and anodizing solution (37% ethanolic HF) were the same for all samples. All samples were etched to a constant charge of 4.5 C/cm^2.

Hérino,[10] higher current densities result in the formation of larger pores (Figure 2).

To obtain information about the pore structure within the porous layer, cross sections of freshly etched samples were imaged by SEM. An image of a porous silicon layer etched at a current density of 440 mA/cm^2 is shown in Figure 3. The image demonstrates that the pores possess a cylindrical (channel-like) structure rather than a network structure as proposed earlier by Smith and Collins[2] and Beale et al.[18]

Adsorption Measurements and Pore Size Distribution. The pore size distributions for the silicon layers etched at low current densities were determined by measurement of adsorption isotherms of nitrogen at 77 K and application of the BJH method.[17] The isotherms obtained from samples etched at 150, 185, and 220 mA/cm^2 exhibit hysteresis loops between the adsorption and desorption branches and are therefore classified as type IV isotherms (de Boer classification, hysteresis loop between branches A and E).[17,19] The isotherms indicate that the materials are mesoporous solids with predominant cylindrically shaped pores. The BJH method used to calculate the pore size distribution takes into account the increasing thickness of the pore walls due to multilayer adsorption of N_2 and describes

(19) (a) IUPAC classification H1. (b) We have not been able to obtain reliable data for the porous silicon wafers (>20 nm pore radius) since our chips were only etched 2−4 μm deep and therefore do not exhibit an absolute surface area large enough to be measured accurately.

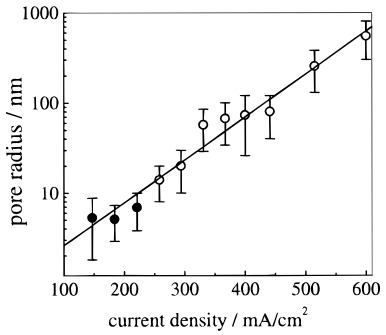

Figure 2. Plot of the logarithm of the measured pore radii vs current density. The values at lower current densities (●) were obtained from BET (Brunnauer−Emmett−Teller) measurements. The values at higher current densities (○) were obtained from SFM measurements. The solid line is a linear least-squares fit to the data. The error bars represent the ranges of the observed radii.

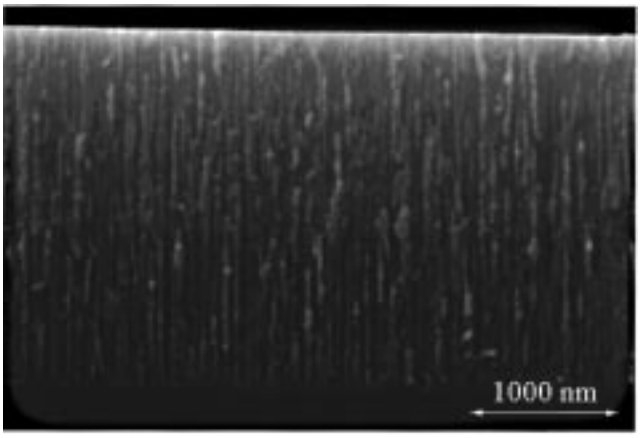

Figure 3. Cross-sectional SEM image of a porous silicon layer etched at 440 mA/cm^2 showing the characteristic cylindrical pore morphology.

the pores as a bundle of cylinders. The pore radii corresponding to the samples anodized at current densities of 150, 185, and 220 mA/cm^2 are in the range 3−10 nm with an absolute surface area of about 0.1−0.15 m^2 for samples etched into a 1 cm^2 patch of silicon. For porous silicon samples prepared at current densities higher than 250 mA/cm^2, the small changes in relative pressure prevent determination of the average pore size using the BET/BJH approach. From the adsorption isotherms it is only obvious that the pore radii are larger than 5 nm.

Hérino et al.[20] successfully applied the BJH method to characterize a variety of n- and p-type porous silicon surfaces. The pore sizes in their study were in the range 3−9 nm. Ruike et al.[21] presented a thorough study of the pore structure of lightly doped p-type porous silicon, obtaining pore radii in the range 1.5−3 nm. Theoretically there is no upper limit to pore sizes that can be obtained by applying the Kelvin equation to the desorption branch of the isotherm. However, an experimental upper limit is imposed for larger pores because the relative pressure changes are very small and therefore difficult to measure accurately. Pores larger than 10 nm in diameter were therefore not measured with this method. Assuming a pore size of 5 nm in diameter, a thickness of about 3500 nm, a porosity of 60%, and a cylindrical pore geometry results in a surface

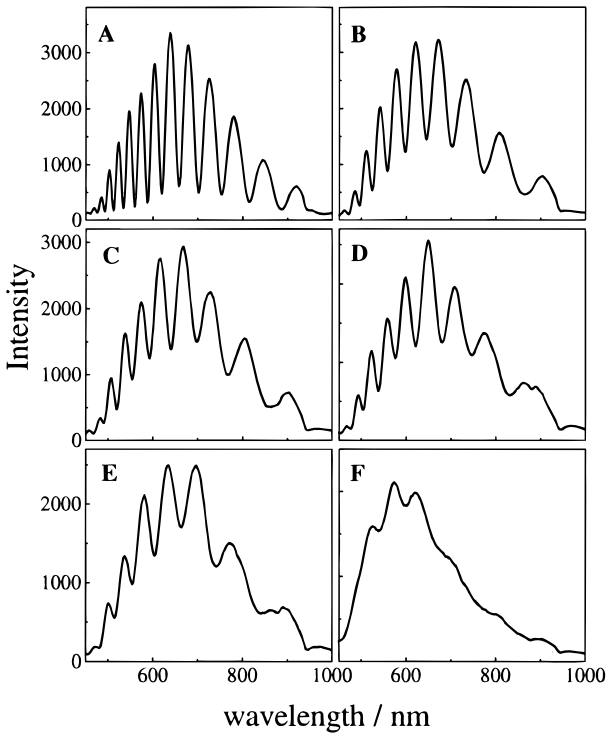

Figure 4. Interference fringe patterns of p-type porous silicon etched at different current densities: (A) 150 mA/cm^2; (B) 295 mA/cm^2; (C) 370 mA/cm^2; (D) 440 mA/cm^2; (E) 515 mA/cm^2; (F) 600 mA/cm^2. All samples were etched to a constant charge of 4.5 C/cm^2. The spectra were taken in the center of the chip.

area of approximately 1000 times the area of a flat smooth surface.[22] This is in good agreement with the surface area obtained from the BET measurements. Similarly, pore radii of 50 nm provide a surface area of only 100 times that of a flat surface. The good agreement between these calculated surface areas and those obtained from BET isotherm measurements supports a cylinder model of the pores even for samples etched at low current densities.

Interferometric Reflectance Spectra. The interference or fringe patterns obtained from porous silicon layers anodized at different current densities are presented in Figure 4. Fabry−Perot fringes using visible light illumination are observed on samples prepared at current densities between 150 and 600 mA/cm^2. Anodization of p-type silicon at a current density of 600 mA/cm^2 results in an obvious matte surface with a barely discernible fringe pattern, due to the increased light scattering occurring at the surface of the upper porous silicon layer. Electropolishing occurs at a current density higher than 700 mA/cm^2. The number of fringes in the observed wavelength range depends on the porosity as well as the thickness of the porous layer. Samples with thicknesses of approximately 3000 nm typically display 9−12 fringes in the 500−1000 nm wavelength region depending on the effective refractive index. The higher the current density, the fewer fringes are observed, consistent with the observation that higher current densities lead to samples with greater porosities. The shape of the curve at lower wavelengths is basically determined by the intensity distribution of the tungsten lamp, while the limited detection range dominates the spectrum at higher wavelengths.[23]

Determination of the Porosity. To determine the porosity p and thickness l of the porous layers, the pores were filled with organic solvents having different refractive indices n. The

(20) Hérino, R.; Bomchil, G.; Barla, K.; Bertrand, C.; Ginoux, J. L. *J. Electrochem. Soc.* **1987**, *134*, 1994.

(21) Ruike, M.; Houzouji, M.; Motohashi, A.; Murase, N.; Kinoshita, A.; Kaneko, K. *Langmuir* **1996**, *12*, 4828.

(22) The thickness of the porous layer was determined by profilometer measurements and the porosity by evaluating the reflectance spectra as described in the Experimental Section.

(23) Theiss, W. *Surf. Sci. Rep.* **1997**, *29*, 91.

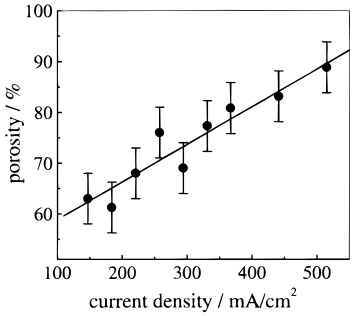

Figure 5. Porosity vs current density plot. The porosities were determined from optical interferometric spectra obtained by filling the porous matrix with different organic solvents of known refractive indices and applying the Looyenga effective medium approximation.

effective optical thickness for each sample was then determined from the interferometric reflectance spectrum. Different effective medium approximations (EMAs) were applied to the data in order to obtain porosity p and thickness l of the porous layer simultaneously. The parameters p and l for each sample were determined from the fit to a plot of $n_{\text{eff}}l$ vs n. Independent of the EMA used, the estimated porosity of porous silicon increases with increasing current density, in close agreement with experimental observation. According to the theory of Looyenga,[24] which assumes a connected silicon network, the porosities are in the range 64−90% (Figure 5). Similar results (57−90%) were obtained using the theory developed by Lazarouk et al.,[25] who assumed void cylinders in a matrix of silicon. However, using the EMA derived by Bruggeman[26] for cylindrical pores as well as Raleigh's theory[27] for a regular array of cylinders with their axes parallel or perpendicular to the field direction, the calculated porosities are significantly lower, in the range 45−73%. The calculated values using the Bruggeman EMA for spheres lead to porosities in the range 58−82%.

To test the validity of the calculated porosities, gravimetric measurements were performed by weighting the sample before and after removal of the porous layer. The gravimetric measurements yielded porosities of 80 ± 5% for porous silicon samples etched at 150 mA/cm^2 and 90 ± 5% for samples etched at 400 mA/cm^2. Compared to the different EMAs used, the Looyenga and the Lazarouk approximations gave values closest to the gravimetrical values. The thicknesses obtained by profilometer and SEM measurements agree best with the thicknesses obtained using the Looyenga and Lazarouk approximation. It should be pointed out that an effective medium approximation is only applicable if the structures embedded in the dielectric matrix are smaller than the wavelength of the light. Thus the porous layers exhibiting very large pores (d > 600 nm) were excluded from the analysis.

Characterization of the Functionalized Porous Silicon Layers. Diffuse reflectance FT-IR spectroscopy was used to monitor the oxidation and functionalization reactions of the porous silicon support. The FT-IR spectrum of the porous silicon layer immediately after anodization of the silicon wafer displays a characteristic broad band centered at 2118 cm^{-1} (Figure 6A) (overlap of the $\nu_{\text{Si-H}_2}$ and $\nu_{\text{H-Si-O}}$ stretching vibrations).[28] The $\nu_{\text{Si-H}}$ and $\nu_{\text{Si-H}_3}$ stretching bands are not visible since backbone oxidation of the Si−Si bonds took place immediately after etching. Oxidation of the porous silicon layer with ozone results in the appearance of the characteristic large and broad Si−O−Si vibrational band around 1110 cm^{-1} in the FT-IR spectrum (Figure 6B). As expected, ozonolysis also leads to complete disappearance of the Si−H vibrational bands. A small band at 887 cm^{-1} assigned to $\delta_{\text{Si-OH}}$ is also observed. Exposure to ozone for longer periods led to complete disappearance of the Si−OH band because the formation of the Si−O−Si bonds is thermodynamically preferred.[2]

After functionalization of the surface with (2-pyridyldithiopropionamidobutyl)dimethylmethoxysilane, the FT-IR spectrum (Figure 6C) displays additional bands characteristic of the linker (the amide A band at 3294 cm^{-1}, the amide I band at 1645 cm^{-1}, the amide II band at 1550 cm^{-1}, the aromatic $\nu_{\text{C-H}}$ band at 3078 cm^{-1}, and the aliphatic $\nu_{\text{C-H}}$ stretching bands at 2954, 2928, and 2864 cm^{-1}).[29] To determine the surface coverage of the immobilized silane linker, the functionalized surface was reduced with dithiothreitol (DTT) to release 2-thiopyridone, which was quantified by UV/vis spectroscopy (λ_{max} = 343 nm, ϵ = 8.08 × 10^3 M^{-1} cm^{-1}).[30] The number of receptor molecules in the case of a silicon chip etched at 440 mA/cm^2 was in the range 20−50 nmol/cm^2, which corresponds to a surface coverage of approximately 30−80%. This calculation is based on the following parameters, assuming cylindrical pores: pore radius, 50 nm; thickness of the porous layer, 3000 nm; porosity, 85%; area per molecule of the biotin linker, 40 Å^2; area of the chip, 1.5 cm^2. The reduction with DDT and subsequent reaction with *N*-[6-(biotinamido)hexyl]-3-(2-pyridyldithio)propionamide (biotin-HPDP) as shown in Scheme 1 led to the desired biotin-functionalized surface which was used in the streptavidin-binding studies (Figure 6D). The band at 1703 cm^{-1} can be assigned to the urea carbonyl stretching vibration of the biotin head group. From the aromatic C−H bands, it can be concluded that some unreacted disulfides remain on the surface. Steric effects are presumably responsible for the incomplete reaction with biotin-HPDP.

Stability of the Porous Silicon Layers in Aqueous Solution. Freshly etched, hydride-terminated porous silicon is unstable in aqueous solutions and will readily suffer oxidative and hydrolytic corrosion. Many applications require a stabilized surface, which has led to the development of various oxidation[31] and derivatization[32] methods for porous silicon. In this study, the stabilities of freshly etched, oxidized, and linker-modified surfaces were investigated. Ethanol (10%, v/v) was included in the phosphate-buffered saline (PBS) solution to allow buffer penetration into the hydrophobic pores of the hydride-terminated and linker-modified samples. As shown in Figure 7, the stability toward corrosion in an aqueous environment varies substantially in the following decreasing order: linker modified ≫ thermally oxidized ≫ ozone oxidized > Si−H terminated. The observed decrease in the normalized effective optical thickness (EOT) with time appears to be caused by oxidation or dissolution of

(24) (a) $n_{\text{eff}}l = [((n_{\text{Si}}l)^{2/3}(1-p) + (nl)^{2/3}p)^3]^{1/2}$; l is the thickness of the porous layer, and n the refractive index of the compound which fills the pores. The refractive index of the bulk silicon is set to n_{Si} = 3.4. (b) Looyenga, H. *Physica* **1965**, *31*, 401.

(25) Lazarouk, S.; Jaguiro, P.; Katsouba, S.; Maiello, G.; Lamonica, S.; Masini, G.; Proverbio, E.; Ferrari, A. *Thin Solid Films* **1997**, *297*, 97.

(26) (a) Bruggeman, D. A. G. *Ann. Phys. (Leipzig)* **1935**, *24*, 636. (b) Since the EMA introduced by Bruggeman can be easily expanded to i components, we used this equation instead of the theory developed by Looyenga to model the dielectric behavior of three-component systems.

(27) Raleigh, J. W. *Philos. Mag.* **1892**, *34*, 481.

(28) (a) Waltenburg, H. N.; Yates, S. T., Jr. *Chem. Rev.* **1995**, *95*, 1589. (b) In the case of less doped p-type porous silicon layers these bands are well resolved: 2117 cm^{-1} for $\nu_{\text{Si-H}_2}$ and 2093/2103 cm^{-1} for $\nu_{\text{H-Si-O}}$.

(29) Krimm, S.; Bandekar, J. *Adv. Protein Chem.* **1986**, *38*, 181.

(30) Stuchbury, T.; Shipton, M.; Norris, R.; Malthouse, J. P. G.; Brocklehurst, K.; Herbert, J. A. L.; Suschitzky, H. *Biochem. J.* **1975**, *151*, 417.

(31) Petrova-Koch, V.; Muschik, T.; Kux, A.; Meyer, B. K.; Koch, F.; Lehmann, V. *Appl. Phys. Lett.* **1992**, 943.

(32) Buriak, J. M.; Allen, M. J. *J. Am. Chem. Soc.* **1998**, *120*, 1339−1443.

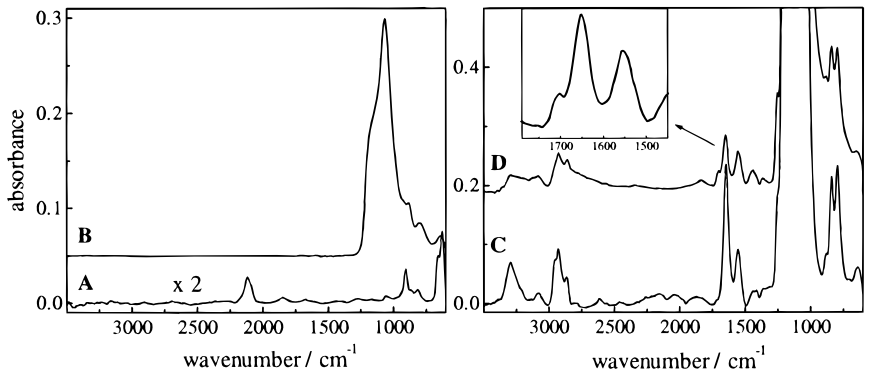

Figure 6. Diffuse reflectance FT-IR spectra of (A) a freshly etched (440 mA/cm^2) p-type porous silicon wafer, (B) the wafer after a 20 min oxidation with ozone, (C) the wafer after functionalization of the porous silicon layer with (2-pyridyldithiopropionamidobutyl)dimethylmethoxysilane, and (D) the wafer after reduction with DDT and subsequent reaction of the free thiols on the surface with biotin-HPDP.

Scheme 1

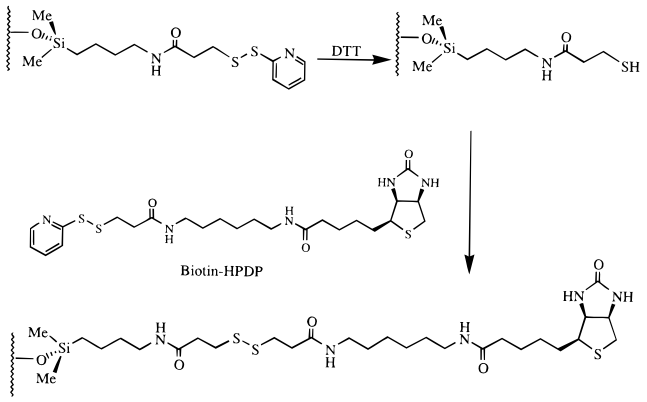

the porous silicon. The conversion of silicon to silica results in a decrease in the effective refractive index of the porous silicon layer, leading to the observed blue shift of the interference fringes. Furthermore, dissolution of the porous layer can lead to a decrease of the thickness of the layer or an increase of the porosity. Both types of dissolution would result in a decrease in the effective optical thickness.

The high stability of the linker-modified surface appears to be due to the capping of oxidation-susceptible sites on the porous silicon surface.[33] The linker-modified surface was synthesized from a silanated ozone-oxidized surface rather than a thermally oxidized surface. Although the thermally treated sample is less susceptible to hydrolytic attack than the ozonolyzed one, significant silation could only be obtained on the ozone-treated sample. The lack of reactivity of thermally oxidized samples appears to be due to the absence of free silanol groups on the thermally treated porous silicon surface. Overall, the linker-modified surface performs two important functions: it protects the porous silicon layer from hydrolysis and provides a modifiable chemical species for subsequent protein−ligand immobilization.

Accessibility of the Porous Matrix. The accessibility of the porous matrix to biological molecules was probed by exposure of a concentrated BSA solution (2.2 mM) in 10 mM PBS buffer to an ozone-oxidized porous silicon sample functionalized with (2-pyridyldithiopropionamidobutyl)dimethylmethoxysilane and pretreated with BSA in order to inhibit nonspecific adsorption to the silicon surface. The measurements were conducted in a home-built flow cell with continuous monitoring (Figure 9; see experimental details). An increase

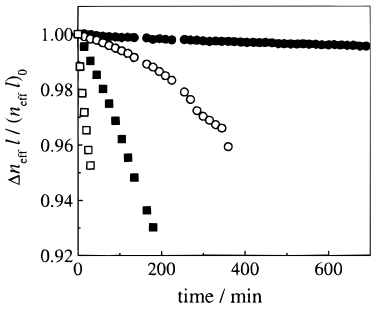

Figure 7. Stability of various surface-derivatized porous silicon samples in 10% (v/v) EtOH in PBS, pH 7.4, presented as the normalized relative effective optical thickness change (normalized EOT) as a function of time. The slopes of $n_{eff}l/t$ are given in brackets: (□) hydride-terminated porous silicon sample [6 nm/min]; (■) ozone-oxidized sample [2 nm/min]; (○) thermally oxidized (400 °C, 1 h) sample [1 nm/min]; (●) ozone-oxidized porous silicon wafer functionalized with (2-pyridyldithiopropionamidobutyl)dimethylmethoxysilane [0.05 nm/min].

in the effective optical thickness of about 10−30 nm was expected considering the volume of the pores and the refractive index of the aqueous BSA solution. The pores were filled with the protein solution within 2−3 min, and the expected equilibrium value of the effective optical thickness was reached after an additional 2 min of incubation (see Supporting Information). This confirms that proteins of this size can enter and fill the porous matrix within a reasonable time scale. Although the observed shift is mainly due to the bulk effect of the protein solution, the slower rate of recovery after rinsing the sample with buffer suggests that some proteins are physisorbed on the silicon walls. Using an ethanol−water mixture (10% ethanol, v/v) instead of the protein solution results in a rectangular signal response upon addition of the mixture ($\Delta n_{eff}l = 11$) and rinsing with water.

Streptavidin Binding to a Biotinylated Porous Silicon Surface. A biotinylated porous silicon surface prepared as described above was exposed to a solution of streptavidin (Figure 8). As expected, specific binding of streptavidin to the biotin-derivatized porous layer resulted in an increase in a red shift of the fringe pattern. This phenomenon is based on the equation $2nl = m\lambda$ for constructive interference of two light beams being reflected at both interfaces of a thin solid-supported transparent film. m is the order of the fringe and λ the wavelength of the incident light hitting the surface with an incident angle of 0°. The change in the effective optical thickness is due to binding of proteins having a higher refractive index than the water in the pores and is in direct quantitative

(33) Pomerantz, M.; Segmueller, A.; Netzer, L.; Sagiv, J. *Thin Solid Films* **1985**, *132*, 153.

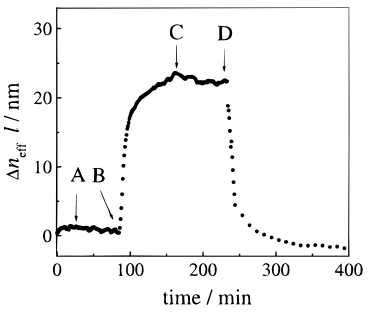

Figure 8. Time course of the effective optical thickness ($n_{eff}l$) of a p-type porous silicon chip etched at 440 mA/cm^2, ozone oxidized for 20 min and functionalized as shown in Scheme 1: (A) addition of 10 μM streptavidin preincubated in 1 mM biotin dissolved in PBS buffer, pH 7.4 (control); (B) addition of 10 μM streptavidin without biotin (washing cycles between); (C) washing cycles with buffer; (D) addition of dithiothreitol, which was used to reduce the disulfide bridge and therefore release the bound protein−linker complex. The sample was mounted in a flow cell with a constant flow rate of 0.5 mL/min.

agreement with what was expected from the effective medium approximations.

As a control, PBS buffer solution containing 10 μM streptavidin which was preincubated in 1 mM biotin (deactivated by saturating all biotin binding sites) does not change the effective optical thickness of the system, suggesting that there is little or no nonspecific protein adsorption to the porous silicon matrix (point labeled A in Figure 8). After a washing cycle with the buffer, a solution containing 10 μM streptavidin (without biotin) was added (assigned as point B in Figure 8), which was immediately detected as an increase in effective optical thickness due to the adsorption of the protein to the biotin receptors immobilized on the porous silicon surface. The overall change in the effective optical thickness ($\Delta n_{eff}l$) after 80 min was 23 nm.

Rinsing the surface with buffer after the protein has bound does not alter the effective optical thickness significantly (arrow C). However, since the biotin recognition element is linked to the surface via a disulfide bond, the protein−ligand complex could be released from the surface by adding dithiothreitol (10 mM) to the bulk phase (arrow D). The initial red shift of 23 nm upon binding streptavidin to the biotinylated porous silicon could be completely reversed, providing further support for the interpretation that the observed red shift is due to the specific binding of the protein to the functionalized surface. Moreover, the reversible linkage of the proteins via disulfide bridges to the surface offers the possibility to reuse the functionalized porous silicon chips for further binding experiments.

The changes in the effective optical thickness expected from a complete protein monolayer can be calculated using a model for the porous surface consisting of an array of closed-packed cylindrical pores. Assuming a thickness of the porous layer of about 2500 nm, a porosity of 80%, and an average pore radius of 80 nm, the amount of protein adsorbed to the pore walls is increased by a factor of approximately 50 compared to that on a flat surface with the same area. Employing the Bruggeman approximation for i components[26]

$$\sum_i f_i \frac{n_i^2 - n_{eff}^2}{n_i^2 - 2n_{eff}^2} = 0 \qquad (1)$$

a rough estimation of the change of the effective refractive index Δn_{eff} upon adsorption of protein can be obtained. f_i denotes the fraction, and n_i is the refractive index of the corresponding component. Solving eq 1 numerically for n_{eff} by setting $n_{Si} = 3.4$, $n_{buffer} = 1.33$, and $n_{protein} = 1.42$, the change in the effective optical thickness ($\Delta n_{eff}l$) due to adsorption of a complete protein monolayer with a thickness of 5 nm is 32 nm. The maximum shifts of about 23 nm observed in the streptavidin/biotin test case are in good agreement with the theoretically calculated value, considering that incomplete coverage of the porous silicon surface with streptavidin occurs because of the expected neighboring steric interactions. Depending on the noise level of the reflectance measurement and the error in extracting the effective optical thickness from the data, the sensitivity of the technique is currently 1−10 ng of protein bound to 1 mm^2 of porous surface, which is equivalent to approximately 5% of a protein monolayer. By decreasing the noise level and using more sophisticated data recording and reduction techniques, one may increase the sensitivity by a factor of 20.

It is noteworthy to point out that the detection mechanism in the present study stands in contrast to that in our previous study of a porous silicon-based biosensor capable of detecting specific adsorption of DNA oligonucleotides to surface-bound complementary DNA, binding of proteins to receptors, and apparent recognition of small molecules by preformed protein layers.[7] Unexpectedly, the adsorption of molecules in the previous study was accompanied by a shift of the spectrum to lower wavelengths, corresponding to a decrease in effective optical thickness. More recent investigation has revealed that surface coverage of the linker was insufficient, leaving most of the material vulnerable to attack by the electrolyte solution, which resulted in oxidation and partial removal of the porous matrix. Presumably, the binding event accelerates degradation of the porous layer by changing the surface potential due to adsorbed charges.[34]

Conclusions

We have demonstrated a simple method for the fabrication of mechanically stable and optically flat porous silicon from heavily doped p-type silicon. The average pore size of the material can be adjusted by varying the etching current density, covering a wide range of pore sizes from a few to several hundred nanometers in diameter. The porosity ranges from 60% to 90%, also depending on the etching current density.

Furthermore, we have shown that the optically flat porous layers exhibit well-resolved interference patterns when illuminated with white light. The sensitivity of the interference patterns toward changes in effective optical thickness of the porous layers was used to monitor the binding of streptavidin to biotin immobilized on the internal surface of the porous silicon layer. Stabilization of the surface against oxidation and corrosion in aqueous media turned out to be crucial and was achieved by ozone oxidation followed by derivatization with a mono-methoxysilane-based biotin linker.

The present study demonstrates that porous silicon can combine the properties of a mechanically and chemically stable high surface area host material with the function of an optical transducer, which makes it an ideal material for biosensing applications. The fact that the system is based on crystalline silicon makes this transducer a prime candidate for integration into high-density sensor arrays and/or micromachined miniaturized systems.

Experimental Section

Etching Procedure. Heavily doped p-type silicon wafers (B-doped, orientation (100)) with a resistivity in the range 0.6−1.0 mΩ cm were used to fabricate porous silicon by an anodic etch in ethanolic HF

(34) Lin, V. S.-Y.; Janshoff, A.; Steinem, C.; Ghadiri, M. R. Manuscript in preparation.

solution (HF:ethanol = 3:1, v/v) prepared from 48% HF in water (Sigma). Prior to the etching procedure, the silicon wafers were rinsed thoroughly with ethanol and dried under a stream of nitrogen. Silicon wafers with an exposed area of 1.5 cm^2 were contacted on the back side with a strip of aluminum foil and mounted in a Teflon etching cell. A platinum mesh served as the counter electrode to provide a homogeneous electrical field. Galvanostatic anodization was performed in the dark with current densities ranging from 150 to 600 mA/cm^2, while the etching time was adjusted to obtain a constant charge in each etched sample of about 4.5 C/cm^2. After etching, the samples were rinsed thoroughly with ethanol and dichloromethane and then dried under a stream of nitrogen.

Oxidation Procedures. The silicon surface was predominant hydride-terminated after the etching procedure. This surface was sensitive to oxidation and hydrolysis upon exposure to aqueous solution. To obtain a surface that was stable in an aqueous buffer, the porous layer was oxidized prior to functionalization. Two different procedures were used to oxidize the surface: ozonolysis and thermal oxidation.

(a) Ozone Oxidation.[35] The freshly etched samples were exposed to ozone for 10 min. The ozone was produced with an ozone generator (Fischer) with a flow rate of 7.7 g/h. After oxidation, the silicon substrates were stored in air.

(b) Thermal Oxidation. Thermally oxidized porous silicon samples were obtained by heat treatment in a furnace tube (Fisher Blue M tube furnace equipped with controller) using the following parameters: initial ramp rate, 5 °C/min to 400 °C; hold time, 1 h; and passive cooling to ambient temperature.

Scanning Force Microscopy. Scanning force microscopy (SFM) images were obtained under ambient conditions using a Nanoscope IIIa Multimode scanning probe microscope (Digital Instruments, Santa Barbara, CA) operating in TappingMode and contact mode. For TappingMode silicon NanoProbe tips (TESP, Digital Instruments) were used as purchased.

Scanning Electron Microscopy. Scanning electron microscopy (SEM) images were obtained with a Cambridge 360 electron microscope using an accelerating voltage of 20 keV. The samples except for the one etched at 600 mA/cm^2 were coated with a thin layer of gold (10 nm) to preclude sample charging.

Determination of the Pore Radius and Surface Area Using BJH and BET Methods. Surface area and pore size distribution were obtained at liquid nitrogen temperature, using a NOVA 1000 apparatus from the Quantachrome Corp. This instrument uses a static volumetric technique. Each sample was outgassed for at least 10 h prior to analysis.

Gravimetry and Profilometry. Two batches of four samples were weighed on a laboratory balance (resolution 10 μg) before and after etching at 150 and 400 mA/cm^2, respectively. The porous layers were then patterned for profilometric analysis by deposition of rows of small droplets of 1 M aqueous NaOH, leading to local dissolution of the porous layer. Profiles were measured on a Dektak II (Veeco/Sloan Technology, Santa Barbara, CA). The remaining porous silicon was dissolved in 1 M aqueous NaOH, and the samples were weighed again. The porosity was calculated as the ratio between the weight loss during the etching and the sum of the weight losses during etching and dissolution in base, respectively.

Interferometric Reflectance Spectra. Interferometric reflectance spectra of porous silicon were recorded by using an Ocean Optics S 1000 spectrometer fitted with a bifurcated fiber optic probe. A tungsten light source was focused onto the center of a porous silicon surface with a spot size of approximately 1−2 mm. Spectra were recorded with a CCD detector in the wavelength range 400−1200 nm. The illumination of the surface as well as the detection of the reflected light was performed along an axis coincident with the surface normal.

The effective optical thickness ($n_{eff}l$) of the porous silicon layer was determined, and the porosity was subsequently calculated by applying an appropriate effective medium approximation (see text). Interference reflectance spectra of the different porous layers were taken in air (n = 1) and after filling the pores with organic solvents differing in their refractive indices: diethyl ether (n = 1.3526), n-hexane (n = 1.3749), tetrahydrofuran (n = 1.4070), and chloroform (n = 1.4459). The effective optical thickness was obtained by using fast Fourier transformation (FFT) of the spectra or from a peak-finding algorithm similar to that proposed by Kraus and Gauglitz.[36] Using a general peak-finding algorithm, we fitted a straight line to the graph of m vs $1/\lambda$. The slope gave the effective optical thickness $n_{eff}l$.

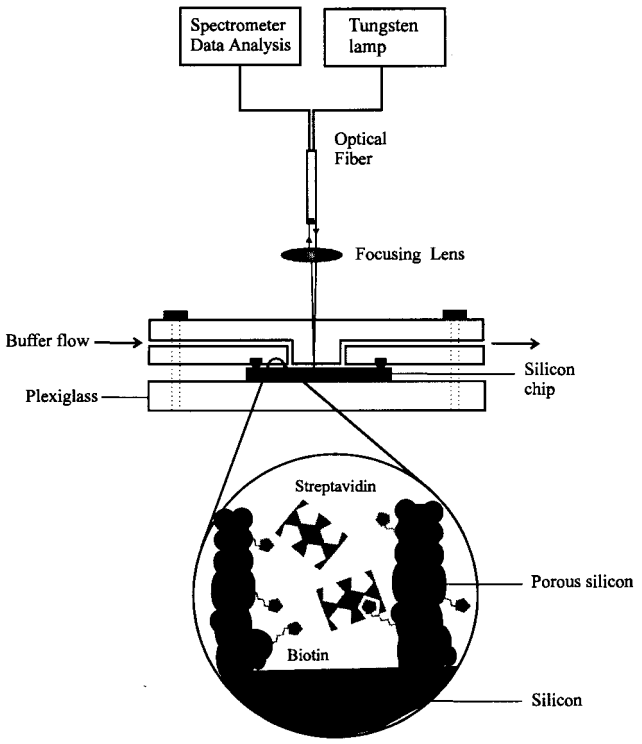

Figure 9. Experimental flow cell and optical interferometer setup used for the stability measurements as well as for the detection of protein−ligand interactions within the pores of a porous silicon layer. A constant flow of approximately 0.5 mL/min was applied by a peristaltic pump.

FT-IR Spectroscopy. FT-IR spectra were acquired with a Nicolet model 550 Magna Series II FT-IR instrument in the diffuse reflectance mode (Spectra-Tech diffuse reflectance attachment), with diffuse reflectance absorption spectra are reported in Kubelka−Munk units. The FT-IR sample compartment was purged with nitrogen.

Functionalization of Oxidized Porous Silicon. (a) Synthesis of (2-Pyridyldithiopropionamidobutyl)dimethylmethoxysilane. 2,2′-Bipyridyl disulfide (3.75 g, 0.017 mol) was dissolved in 15 mL of ethanol (99.5%), and 0.4 mL of glacial acetic acid was added. The solution was stirred vigorously, and 0.9 g (8.5 mmol) of 3-mercaptopropionic acid in 5 mL of ethanol was added dropwise. The reaction mixture was allowed to stir at room temperature for 12 h. Solvent was then removed by evaporation. The resulting oily product mixture was dissolved in 10 mL of methylene chloride/ethanol (3:2, v/v). The product was purified by neutral alumina column chromatography. The pyridine-2-thione eluted as a yellow band. The desired product remained adsorbed to the alumina on the top of the column. A few milliliters of glacial acetic acid (10 mL/250 mL of methylene chloride/ethanol eluent) was added to the eluent mixture. The other side product (2,2′-dicarboxyethyl disulfide) was retarded on the column and thus separated from the desired product (2-pyridyl-2-carboxyethyl disulfide). The product was collected, and the solvent was removed by evaporation. The residual acetic acid was removed under high vacuum. Isolated yield = 1.5 g (82.2%, based on 0.9 g of the 3-mercaptopropionic acid starting material).

The isolated product (2-pyridyl-2-carboxyethyl disulfide) was quickly dissolved in a methylene chloride solution (100 mL). 1-(3-(Dimethylamino)propyl)-3-ethylcarbodiimide hydrochloride (EDC) (668 mg, 3.5 mmol) was added to the solution. The resulting solution was allowed

(35) (a) Kazor, A.; Gwilliam, R.; Boyd, I. W. *Appl. Phys. Lett.* **1994**, *65*, 412. (b) Chao, S. C.; Pitchai, R.; Lee, Y. H. *J. Electrochem. Soc.* **1989**, *136*, 2751. (c) Thompson, W. H.; Yamani, Z.; Abu Hassan, L. H.; Greene, J. E.; Nayfeh, M. *J. Appl. Phys.* **1996**, *80*, 5415.

(36) Kraus, G.; Gauglitz; G. *Fresenius' J. Anal. Chem.* **1992**, *344*, 153.

to stir under N_2 for 30 min before (4-aminobutyl)dimethylmethoxysilane (0.65 mL, 3.5 mmol) was added by syringe. The reaction mixture was stirred vigorously at room temperature for 12 h, and the reaction was quenched with saturated $NaHCO_3$ aqueous solution. The organic layer was extensively washed and extracted from the aqueous layer. The solution was then dried over sodium carbonate (anhydrous) and filtered, and the methylene chloride was removed by evaporation to yield a pale-yellow oil. The product was repurified by silica chromatography with ethyl acetate as eluent. Isolated yield = 1.2 g (85%, based on 1.5 g of the 2-pyridyl-2-carboxyethyl disulfide starting material). ^{1}H NMR (250 MHz, $CDCl_3$): δ 8.32 (m, 1H), 7.54 (m, 2H), 7.01 (m, 1H), 3.32 (s, 3H), 3.14 (m, 2H), 2.95 (t, 2H, J = 6.8 Hz), 2.48 (t, 2H, J = 6.9 Hz), 1.44 (m, 2H), 1.25 (m, 2H), 0.50 (m, 2H), −0.02 (s, 6H).

(b) Functionalization of the Porous Layers. The porous silicon samples were functionalized by refluxing them in a 50 mM solution of (2-pyridyldithiopropionamidobutyl)dimethylmethoxysilane dissolved in toluene for 12 h. After functionalization, the samples were rinsed successively with toluene, ethanol, water, and acetone and subsequently dried under a stream of nitrogen. The functionalized porous silicon samples were then incubated in an aqueous solution of dithiothreitol (10 mM) for 1 h to reduce the disulfide. After extensive rinsing with water, 0.5 mL of a stock solution of 2 mg/mL of biotin-HPDP (Pierce) in DMSO was mixed with 0.5 mL of PBS buffer, the resulting solution was added to each porous silicon chip, and the sample was incubated for 30 min. Afterward, the chip was washed 5 times with 2 mL of DMSO, 5 times with 2 mL of DMSO/water (1:1), 5 times with 2 mL of DMSO, and 5 times with PBS/Triton X (0.1%, v/v). The release of the thiopyridyl group by forming the disulfide was checked by UV/vis spectroscopy (λ_{max} at 340 nm).

Stability Measurements. All stability studies were performed on p-type silicon etched at 440 mA/cm^2. Hydride-terminated porous silicon samples were used immediately following their fabrication. Each sample was mounted into a flow cell as depicted in Figure 9 and exposed to 10% EtOH (v/v) in PBS, pH 7.4, at a flow rate of 0.4 mL/min. Interference spectra were acquired every 5 min for the hydride-terminated samples and every 15 min for all other samples.

Protein Binding. Streptavidin binding to a biotinylated surface was carried out in a flow cell as depicted in Figure 9 in a PBS buffer containing 0.1% Triton X. The cell consisting of plexiglass was connected via an inlet and an outlet to a peristaltic pump. The light beam was focused on the surface of the sample through the plexiglass cover. A constant buffer flow of 0.5 mL/min was maintained. Interference spectra were recorded, and the effective optical thickness was obtained by FFT.

Acknowledgment. We thank the office of Naval Research (Grants N00014981073 and N000149511293) through the Multidisciplinary University Research Initiative (Grant MURI-95) of the Department of Defense for financial support of this work. We also thank the Fonds der Chemischen Industrie (A.J.), the DFG (C.S.), the National Institutes of Health (K.-P.S.D. and K.M.), and the Skaggs Research Institute (V.S.-Y.L.) for postdoctoral fellowships.

Supporting Information Available: Additional SFM procedures, magnifications of SFM images, SEM top and cross-sectional views of porous silicon, BET isotherm and pore size distribution plots for a porous silicon chip, the reflectance spectrum of a porous silicon layer along with a data reduction procedure, and a figure showing the reversible penetration of BSA in the pores measured by interference reflectance spectroscopy (9 pages, print/PDF). See any current masthead page for ordering information and Web access instructions.

JA9826237